

**Enabling Multifunctional Electrocatalysts by Modifying the Basal Plane of
Unifunctional 1T'-MoS₂ with Anchored Transition-Metal Single Atoms**

Yuanyuan Wang¹, Mengru Wang,¹ Zhansheng Lu², Dongwei Ma^{1,*}, and Yu Jia^{1,3*}

¹*Key Laboratory for Special Functional Materials of Ministry of Education, and School of
Materials Science and Engineering, Henan University, Kaifeng 475004, China*

²*School of Physics, and National Demonstration Center for Experimental Physics Education,
Henan Normal University, Xinxiang 453007, China*

³*International Laboratory for Quantum Functional Materials of Henan, and School of
Physics and Engineering, Zhengzhou University, Zhengzhou 450001, China*

Supporting Information

*Corresponding author. E-mail: madw@henu.edu.cn (D. Ma).

*Corresponding author. E-mail: jiayu@henu.edu.cn (Y. Jia).

Table S1. The zero-point energy (E_{ZPE} in eV) and entropy (TS) corrections to the free energy for the relevant gas molecules and intermediates.

Species	E_{ZPE}	TS
$H_2O(l)$	0.56	0.67
$H_2(g)$	0.27	0.41
O^*	0.06	0.07
OH^*	0.35	0.10
OOH^*	0.45	0.18
H^*	0.21	0.01
*	0.00	0.00

Table S2. Theoretical overpotentials of the OER (η_{OER}) and ORR (η_{ORR}), and the solvation energy (in eV) of the intermediates (OH^* , O^* , and OOH^*) on $Co@MoS_2$ calculated with different combinations of the width of the dielectric cavity (SIGMA_K flag in VASP) and the cutoff charge density (NC_K flag in VASPsol). The solvation energy (in eV) is defined by $\Delta E_{sol} = E_{sol} - E_{vacuum}$, where E_{sol} and E_{vacuum} are the total energies of the systems with and without solvation included, respectively. It is found that with increase in NC_K and SIGMA_K, overall, the solvation energies become more negative, and thus the intermediates are more stabilized due to the solvation effect. However, too large NC_K or SIGMA_K can lead to unrealistic stability of the intermediates. The similar trend has been observed in Ref.¹. On the other hand, interestingly we can see that the changes in the predicted theoretical overpotentials with the different combinations of NC_K and SIGMA_K are small compared with the default parameters (NC_K = 0.0025 and SIGMA_K = 0.6).

(NC_K, SIGMA_K)	$\Delta E_{sol}(OH^*)$	$\Delta E_{sol}(O^*)$	$\Delta E_{sol}(OOH^*)$	η_{OER}	η_{ORR}
(0.0025, 0.6000)	-0.07	0.00	-0.10	0.28	0.26
(0.0045, 0.6000)	-0.38	-0.25	-0.43	0.33	0.30
(0.0080, 0.6000)	-1.38	-1.16	-1.76	0.43	0.40
(0.0025, 0.8000)	-0.30	-0.19	-0.34	0.32	0.30
(0.0025, 1.0000)	-1.20	-1.03	-1.28	0.37	0.34
(0.0045, 0.8000)	-1.25	-1.06	-1.36	0.40	0.35

Table S3. Solvation energy (in eV) for the ORR and OER intermediates (OH^* , O^* , and OOH^*) on Co@MoS_2 , Rh embedded N-doped graphene (Rh@Gr)², and one-dimensional Co dithiolene (Co-D)³. Note that the explicit and implicit corrections have been adopted for Rh@Gr and Co-D SACs, respectively. The default parameters in VASPsol give the solvation energies for OH^* , O^* , and OOH^* on the Co@MoS_2 systems of -0.07, 0.00, and -0.10 eV, respectively. These values are close to the results ($\Delta E_{\text{sol}}(\text{OH}^*) = -0.20$ eV, $\Delta E_{\text{sol}}(\text{O}^*) = 0.00$ eV, and $\Delta E_{\text{sol}}(\text{OOH}^*) = -0.10$ eV) by explicit solvation model for Rh@Gr as SACs², and the results ($\Delta E_{\text{sol}}(\text{OH}^*) = -0.15$ eV, $\Delta E_{\text{sol}}(\text{O}^*) = -0.09$ eV, and $\Delta E_{\text{sol}}(\text{OOH}^*) = -0.22$ eV) by the implicit solvation model for the Co-D as SACs³. We notice that the latter reference³ used the default parameters for VASPsol. Considering the consistency between our results and those in above two references, we also used default parameters for VASPsol to include the solvation effect.

	$\Delta E_{\text{sol}}(\text{OH}^*)$	$\Delta E_{\text{sol}}(\text{O}^*)$	$\Delta E_{\text{sol}}(\text{OOH}^*)$
Co@MoS_2	-0.07	0.00	-0.10
Rh@Gr	-0.20	0.00	-0.10
Co-D	-0.15	-0.09	-0.22

Table S4. The calculated solvation energy ($\Delta E_{\text{sol}} = E_{\text{sol}} - E_{\text{vacuum}}$, in eV) of the intermediates for ORR and OER (OH^* , O^* , and OOH^*) on the various catalysts.

	$\Delta E_{\text{sol}}(\text{OH}^*)$	$\Delta E_{\text{sol}}(\text{O}^*)$	$\Delta E_{\text{sol}}(\text{OOH}^*)$
Ti@MoS ₂	-0.11	-0.05	-0.21
V@MoS ₂	-0.16	-0.08	-0.24
Cr@MoS ₂	-0.12	-0.06	-0.19
Mn@MoS ₂	-0.12	-0.04	-0.22
Fe@MoS ₂	-0.13	-0.05	-0.20
Co@MoS ₂	-0.07	0.00	-0.10
Ni@MoS ₂	-0.05	-0.02	-0.19
Cu@MoS ₂	-0.11	-0.10	-0.16
Mo@MoS ₂	-0.05	-0.03	-0.18
Ru@MoS ₂	-0.09	-0.03	-0.12
Rh@MoS ₂	-0.07	-0.05	-0.24
Pd@MoS ₂	-0.06	-0.06	-0.14
Os@MoS ₂	-0.11	0.00	-0.21
Ir@MoS ₂	-0.12	-0.05	-0.23
Pt@MoS ₂	-0.09	0.00	-0.14

Table S5. The calculated adsorption energies (in eV) for the various TM single atoms at the considered adsorption sites on the 1T'-MoS₂ monolayer. For the top sites of the S atoms, in almost all cases the TM atoms, after structural relaxation, diffuse to their neighboring sites. The most stable sites are emphasized in bold.

Systems	H _{T1}	H _{T2}	M _{T1}	M _{T2}	S _{T1}	S _{T2}
Ti@MoS ₂	-6.23	-6.60	-5.79	-6.01	H _{T1}	M _{T2}
V@MoS ₂	-5.61	-5.76	-4.80	-5.13	H _{T1}	-2.35
Cr@MoS ₂	-3.40	-3.95	-3.39	-3.82	H _{T1}	M _{T2}
Mn@MoS ₂	-3.62	-3.87	-3.58	-3.94	M _{T1}	M _{T2}
Fe@MoS ₂	-4.53	-4.87	-4.22	-4.55	H _{T1}	M _{T2}
Co@MoS ₂	-4.71	-5.31	-4.54	-4.87	H _{T1}	M _{T2}
Ni@MoS ₂	-4.29	-4.74	-4.34	-4.73	H _{T1}	M _{T2}
Cu@MoS ₂	-3.03	-3.18	-3.11	-3.47	H _{T1}	M _{T2}
Mo@MoS ₂	-5.86	-5.07	-4.99	-4.99	H _{T1}	M _{T2}
Ru@MoS ₂	-5.43	-5.81	-5.13	-5.42	H _{T1}	M _{T2}
Rh@MoS ₂	-4.25	M _{T2}	-4.43	-4.90	H _{T1}	M _{T2}
Pd@MoS ₂	-2.72	M _{T2}	-3.02	-3.45	H _{T1}	M _{T2}
Os@MoS ₂	-6.43	-6.25	-6.18	-6.34	H _{T1}	-2.35
Ir@MoS ₂	-5.31	-5.74	-5.20	-5.41	H _{T1}	-2.73
Pt@MoS ₂	-3.78	M _{T2}	-3.98	-4.57	H _{T1}	-3.02

Table S6. The TM-S bond lengths (in Å) for all the TM@MoS₂ systems. The adsorption sites for the specific TM atoms are also displayed in the first column. $d_{\text{TM-Sn}}$ (n = 1, 2, 3, and 4) denotes the bond length between the TM atom and its neighboring S atoms (S1, S2, S3, and S4), which can be seen in Fig. S2.

	$d_{\text{TM-S1}}$	$d_{\text{TM-S2}}$	$d_{\text{TM-S3}}$	$d_{\text{TM-S4}}$
Ti@MoS ₂ (H _{T2})	2.19	2.19	2.24	2.50
V@MoS ₂ (H _{T2})	2.13	2.13	2.45	2.34
Cr@MoS ₂ (H _{T2})	2.13	2.13	2.18	2.28
Mn@MoS ₂ (M _{T2})	2.26	2.26	2.34	--
Fe@MoS ₂ (H _{T2})	2.11	2.11	2.20	2.41
Co@MoS ₂ (H _{T2})	2.08	2.08	2.15	2.16
Ni@MoS ₂ (M _{T2})	2.10	2.10	2.24	--
Cu@MoS ₂ (M _{T2})	2.20	2.20	2.28	--
Mo@MoS ₂ (H _{T1})	2.30	2.30	2.48	2.32
Ru@MoS ₂ (H _{T2})	2.18	2.18	2.23	2.29
Rh@MoS ₂ (M _{T2})	2.21	2.21	2.34	--
Pd@MoS ₂ (M _{T2})	2.29	2.29	2.47	--
Os@MoS ₂ (H _{T1})	2.29	2.29	3.35	2.27
Ir@MoS ₂ (H _{T2})	2.22	2.22	2.32	2.27
Pt@MoS ₂ (M _{T2})	2.23	2.23	2.50	--

Table S7. The change of the S-Mo bond length (in Å) due to the adsorption of the TM single atoms on the 1T'-MoS₂ monolayer. The definition of the Δd_n (n = 1-9) can be seen from Fig. S3. The adsorption sites for the specific TM atoms are also displayed in the first column.

	Δd_1	Δd_2	Δd_3	Δd_4	Δd_5	Δd_6	Δd_7	Δd_8	Δd_9
Ti@MoS ₂ (H _{T2})	-0.02	0.24	0.36	-0.02	0.24	0.36	0.25	-0.10	0.25
V@MoS ₂ (H _{T2})	0.03	0.33	0.22	0.03	0.33	0.22	0.21	-0.07	0.21
Cr@MoS ₂ (H _{T2})	0.01	0.24	0.37	0.01	0.24	0.37	0.26	-0.08	0.26
Fe@MoS ₂ (H _{T2})	0.01	0.30	0.17	0.01	0.30	0.17	0.23	-0.08	0.23
Co@MoS ₂ (H _{T2})	0.01	0.31	0.10	0.01	0.31	0.10	0.21	-0.08	0.21
Ru@MoS ₂ (H _{T2})	0.01	0.32	0.51	0.01	0.32	0.51	0.35	-0.08	0.35
Ir@MoS ₂ (H _{T2})	0.04	0.62	0.13	0.04	0.62	0.13	0.27	-0.09	0.27
Mo@MoS ₂ (H _{T1})	0.05	1.78	0.06	0.05	1.78	0.06	0.01	0.04	0.01
Os@MoS ₂ (H _{T1})	0.03	1.32	0.07	0.03	1.32	0.07	0.07	0.00	0.07
Mn@MoS ₂ (M _{T2})	0.02	0.09	0.02	0.02	0.09	0.02	0.04	0.02	0.04
Ni@MoS ₂ (M _{T2})	0.01	0.15	0.01	0.01	0.15	0.01	0.01	0.02	0.01
Cu@MoS ₂ (M _{T2})	-0.01	0.11	0.00	-0.01	0.11	0.00	0.01	0.04	0.01
Rh@MoS ₂ (M _{T2})	0.03	0.16	0.03	0.03	0.16	0.03	0.01	0.04	0.01
Pd@MoS ₂ (M _{T2})	0.01	0.15	0.00	0.01	0.15	0.00	-0.01	0.04	-0.01
Pt@MoS ₂ (M _{T2})	0.01	0.26	0.01	0.01	0.26	0.01	-0.01	0.03	-0.01

Table S8. The spin magnetic moments (M in μ_B) localized on the embedded TM atoms and the work function (Φ in eV) of the various $\text{TM}@\text{MoS}_2$. The calculated work function for the pristine 1H-MoS₂ (5.85 eV) and 1T'-MoS₂ (5.75 eV) monolayers are in good agreement with the values in references (5.96 eV for 1H-MoS₂⁴ and \sim 5.5 eV for 1T'-MoS₂⁵).

	M	Φ
Ti@MoS ₂	0.00	5.53
V@MoS ₂	0.00	5.57
Cr@MoS ₂	1.95	5.61
Mn@MoS ₂	4.28	5.55
Fe@MoS ₂	2.43	5.63
Co@MoS ₂	0.00	5.62
Ni@MoS ₂	0.00	5.67
Cu@MoS ₂	0.00	5.60
Mo@MoS ₂	0.00	5.59
Ru@MoS ₂	0.00	5.62
Rh@MoS ₂	0.00	5.65
Pd@MoS ₂	0.00	5.65
Os@MoS ₂	0.00	5.71
Ir@MoS ₂	0.00	5.60
Pt@MoS ₂	0.00	5.65
1T'-MoS ₂		5.75
1H-MoS ₂		5.85

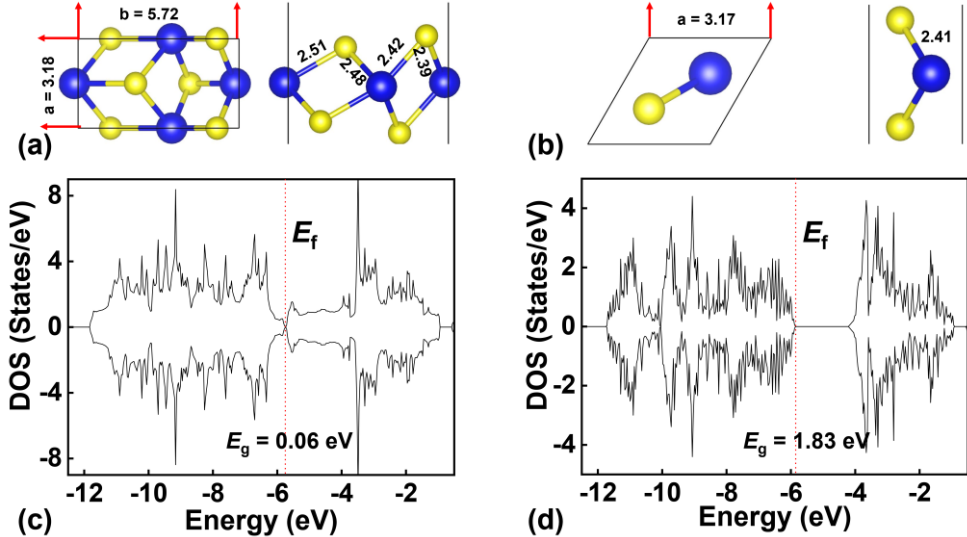


Fig. S1. The atomic structures of the unit cells of 1T'-MoS₂ (a) and 1H-MoS₂ (b) monolayers, and the densities of states (DOS) of the 1T'-MoS₂ (c) and 1H-MoS₂ (d) monolayers. In (a) and (b), yellow and blue spheres denote S and Mo atoms, respectively, and the lattice parameters (in Å) and the lengths (in Å) of the Mo-S bonds are given. In (c) and (d), the positive and negative DOS denote the spin-up and spin-down states, respectively. The Fermi level (E_f) is indicated by the dashed vertical line, which is aligned with respect to the vacuum level. Note that the optimized geometric structures and the calculated DOS for both phases are in good agreement with previous studies. In detail, for 1H-MoS₂, the calculated lattice parameter ($a = 3.17$ Å), the Mo-S bond length ($d_{\text{Mo-S}} = 2.41$ Å), and the band gap ($E_g = 1.83$ eV) are in good agreement with the theoretical values of $a = 3.20$ Å, $d_{\text{Mo-S}} = 2.42$ Å, and $E_g = 1.58$ eV.⁴ Note the experimental band gap of the 1H-MoS₂ monolayer is about 1.8 eV.⁶ For 1T'-MoS₂, the calculated lattice parameters ($a = 3.18$ Å and $b = 5.72$ Å) and the band gap ($E_g = 0.06$ eV) agree well with the theoretical values of $a = 3.22$ Å and $b = 5.81$ Å and $E_g = \sim 0.1$ eV, indicating the semi-metallic property of 1T'-MoS₂.⁷ In addition, the calculated work functions for both phases are also in good agreement with previous works, as discussed in Table S8.

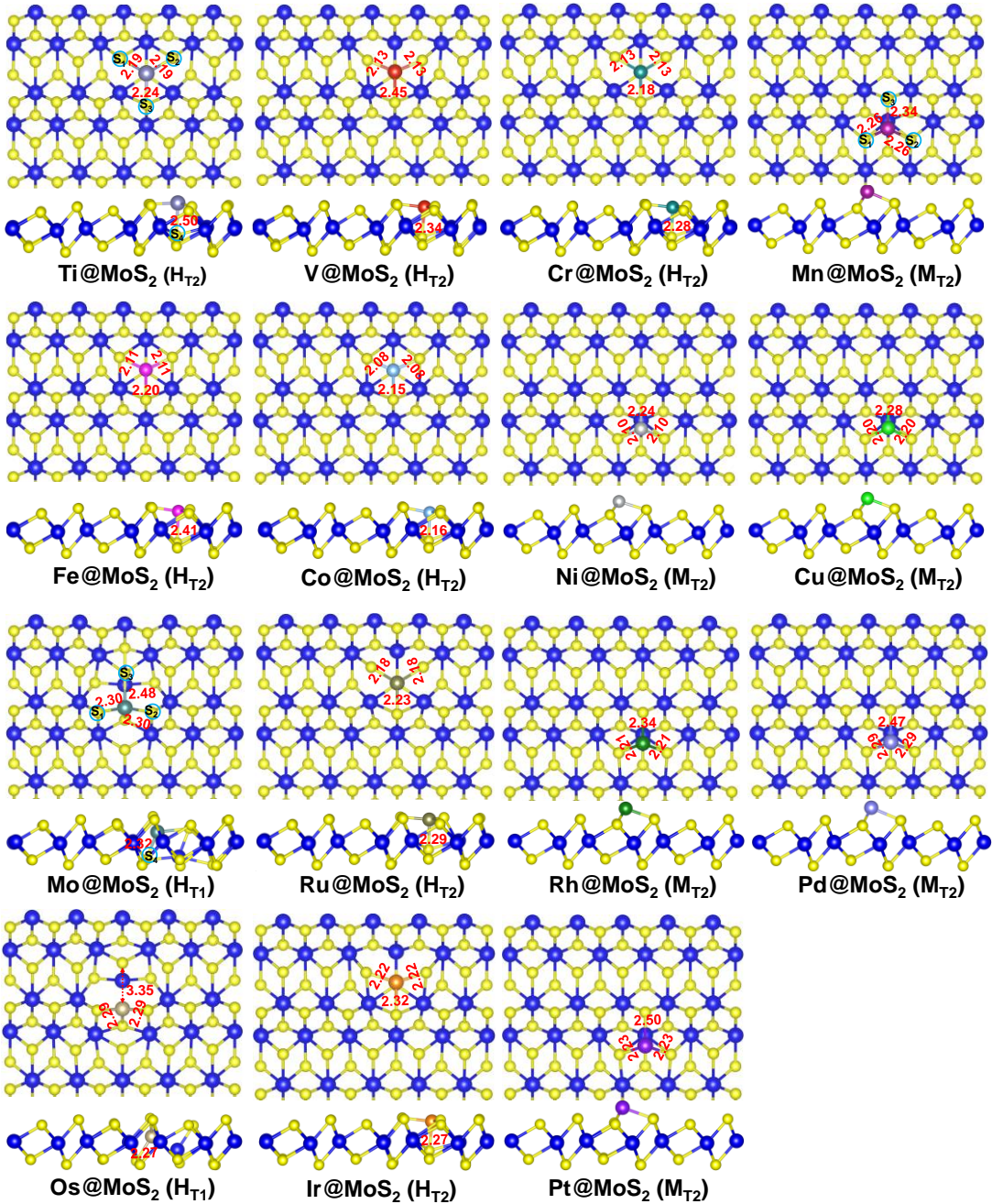


Fig. S2. The top and side views of the various TM@MoS₂ SACs. The distances (in Å) between the anchored TM atom and its neighboring S atoms are presented. For S1, S2, S3, and S4 atoms, one can refer to Ti@MoS₂ for H_{T2} site, Mn@MoS₂ for M_{T2} site, and Mo@MoS₂ for H_{T1} site.

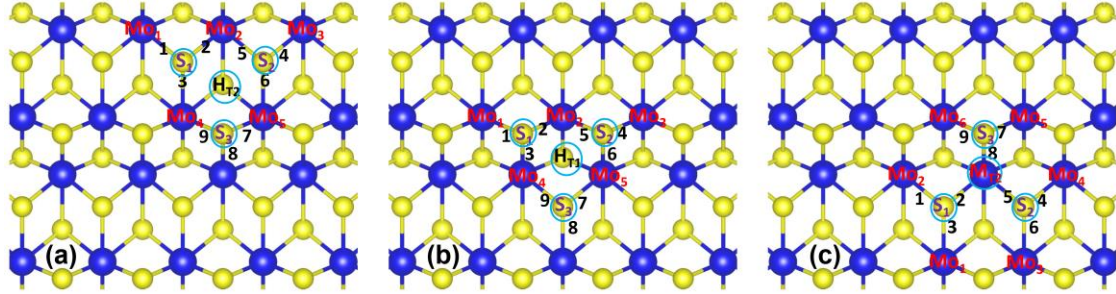


Fig. S3. The H_{T2} , H_{T1} , and M_{T2} adsorption sites for the TM single atoms on the 1T'- MoS_2 monolayer are marked in (a), (b), and (c), respectively. The $S1$, $S2$, and $S3$ atoms are the three S atoms neighboring the adsorbed TM atoms. The numbers in the figures indicate the S-Mo bond. For example, in (a), 1 denotes the bond between S_1 and Mo_1 , and the corresponding bond length (in Å) is represented as d_1 . Further, the difference between this bond length and the corresponding S-Mo bond length in the pristine 1T'- MoS_2 monolayer is represented as Δd_1 .

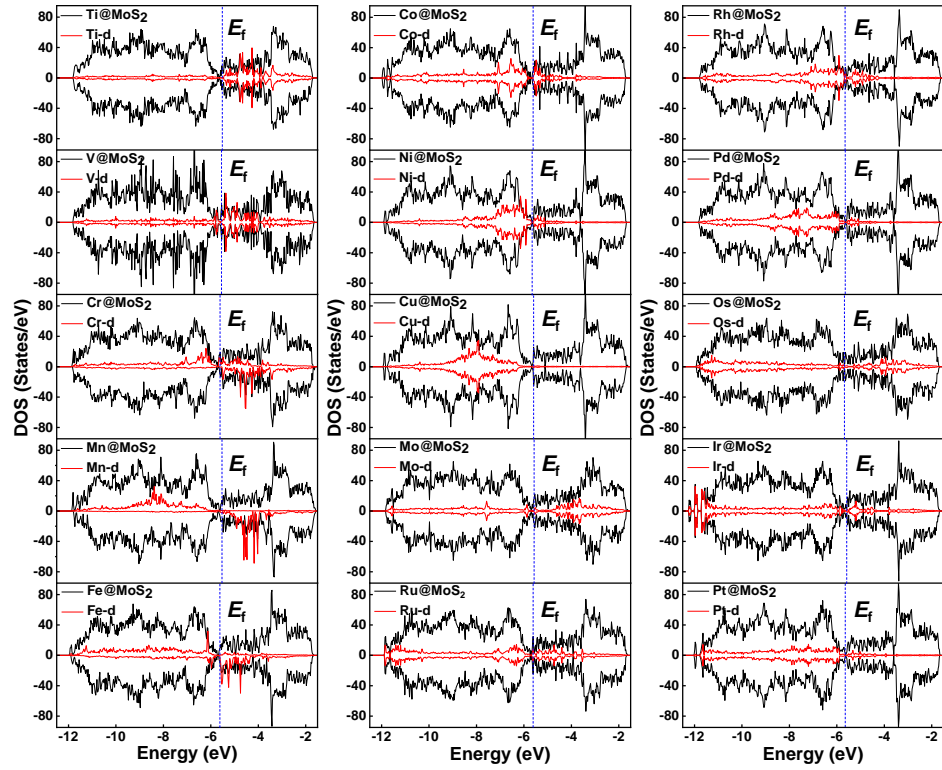


Fig. S4. The total DOS (black line) and local DOS (red line) of the d states of the anchored TM atoms for TM@MoS₂. The Fermi level is indicated by the vertical dashed line, with respect to the vacuum level.

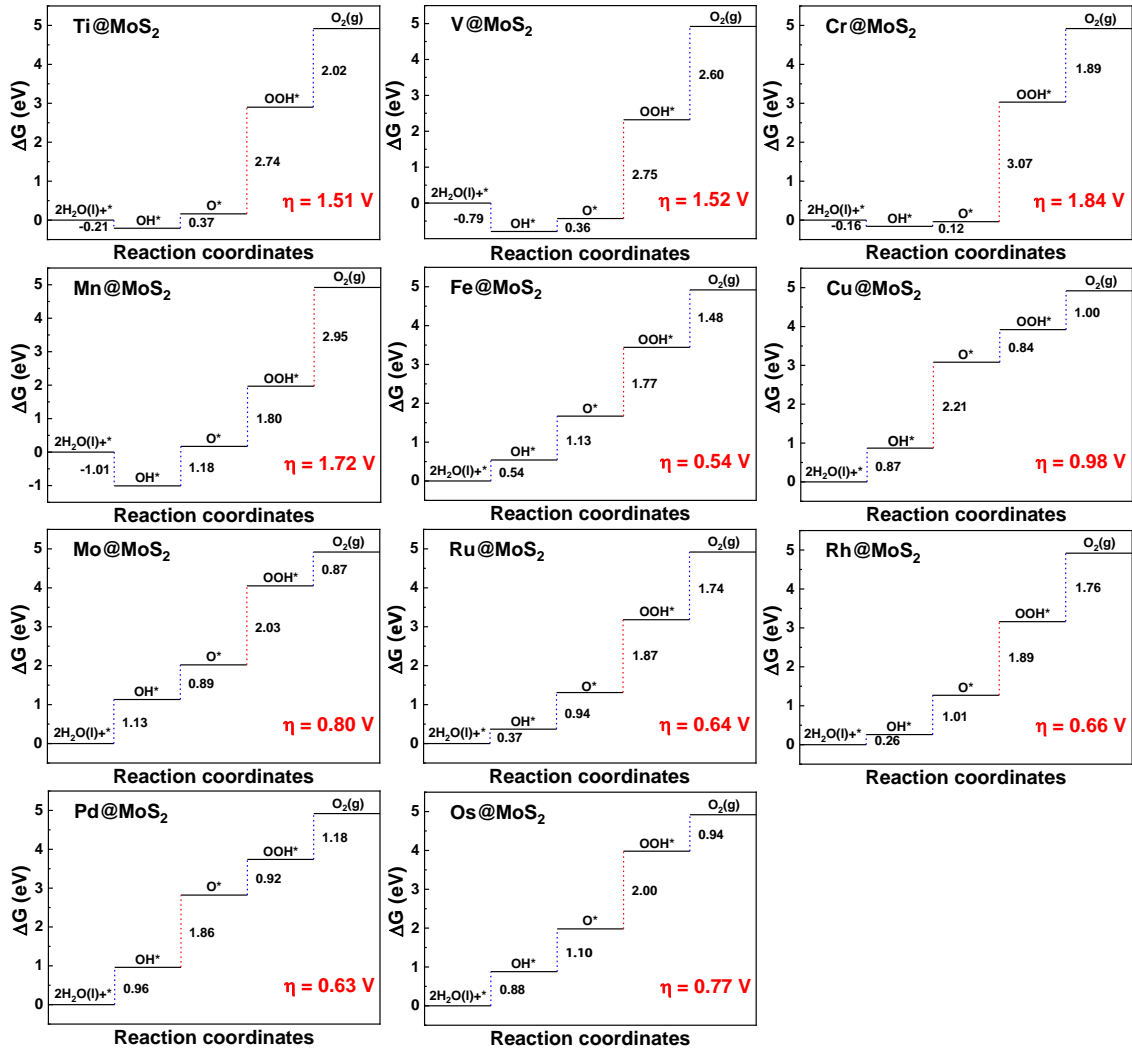


Fig. S5. The Gibbs free energy diagrams under zero potential for the OER on the various TM@MoS₂ SACs.

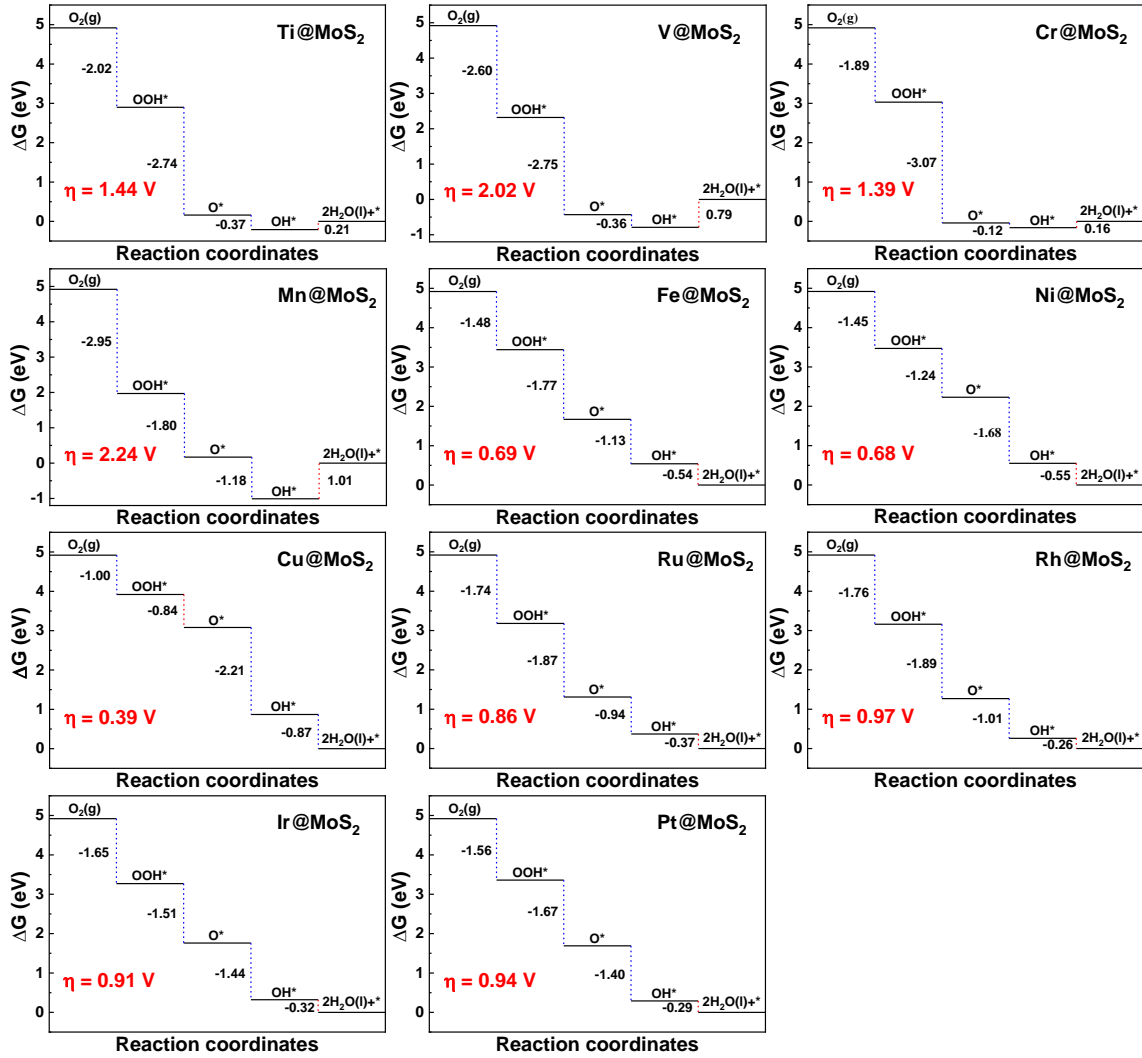


Fig. S6. The Gibbs free energy diagrams under zero potential for the ORR on the various TM@MoS₂ SACs.

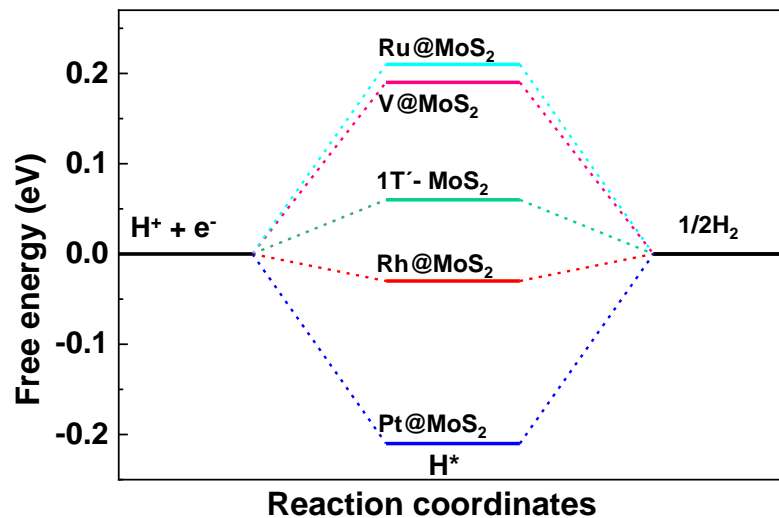


Fig. S7. The Gibbs free energy diagrams under zero potential for the HER on the pristine 1T'-MoS₂, and Ru, V, Rh, and Pt@MoS₂.

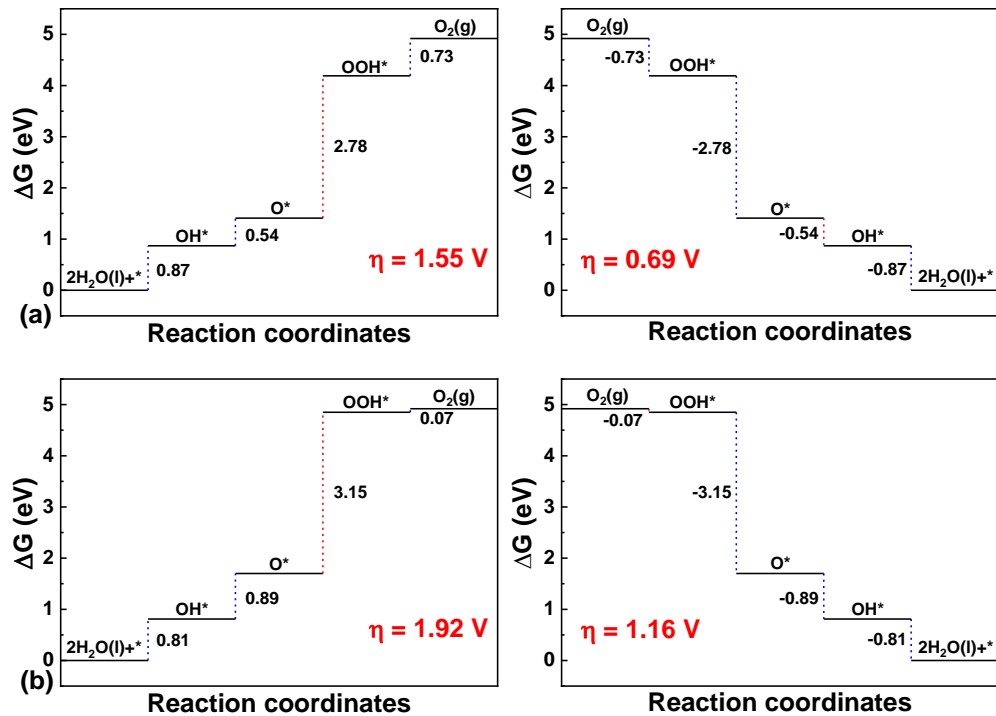


Fig. S8. The Gibbs free energy diagrams under zero potential for the OER and ORR at the S_{T1} (a) and S_{T2} (b) sites, as shown in Fig. 1a.

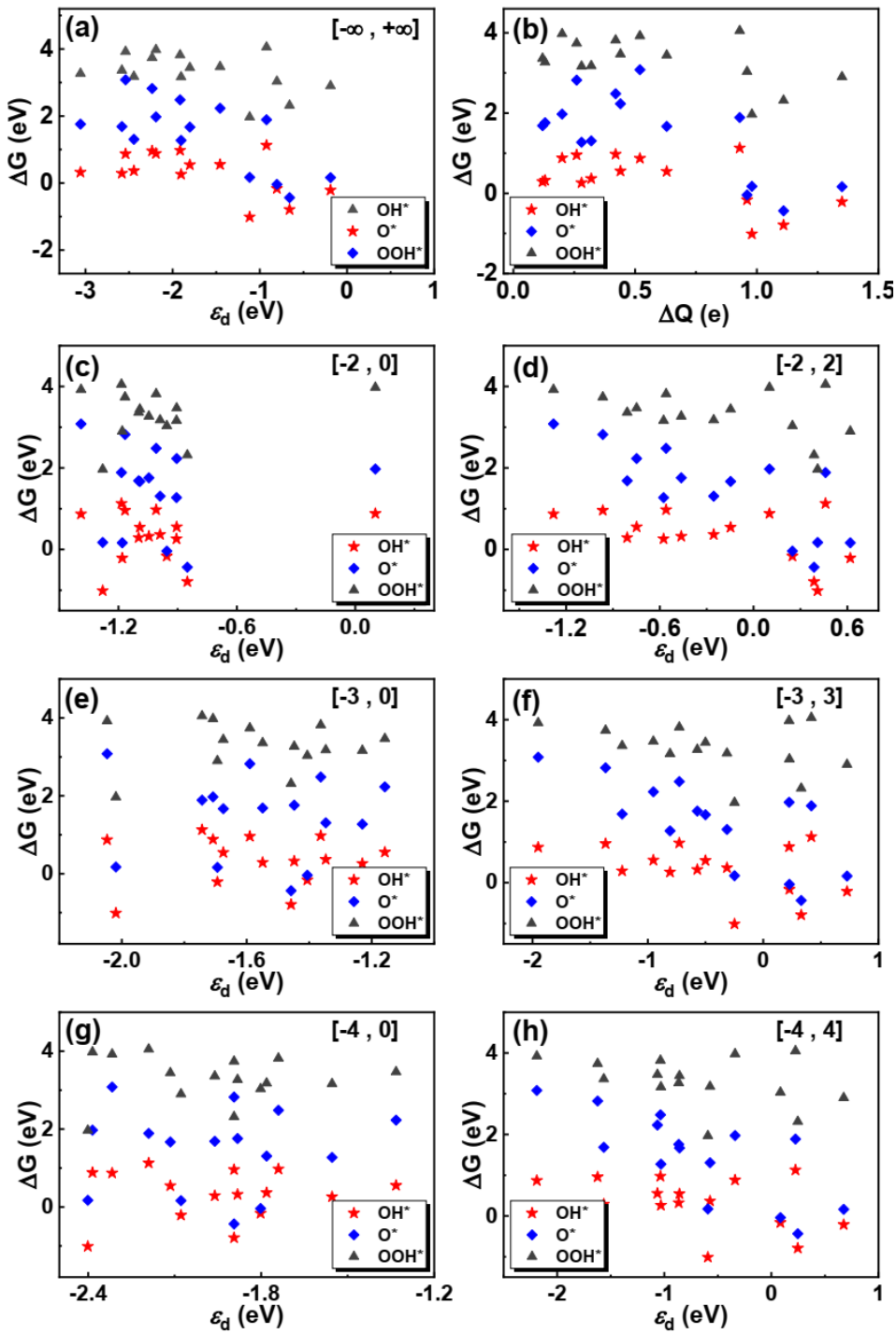


Fig. S9. The relationship between the binding strengths of the reaction intermediates and the d-band center (ε_d) or the net charges (ΔQ) of the supported TM atoms in the bare TM@MoS₂. For the d-band center, various integral bounds have been considered.

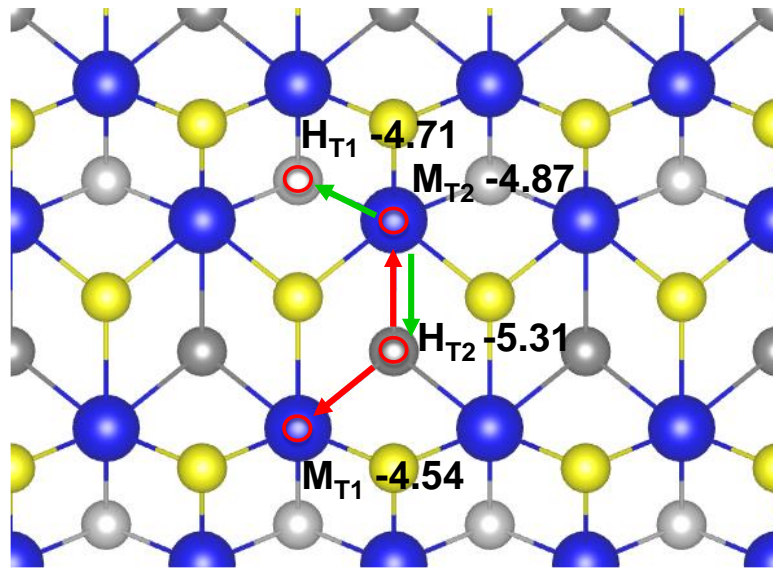


Fig. S10. The possible diffusion paths for the Co single atom on the 1T'-MoS₂, with the adsorption energies displayed for the specific adsorption sites.

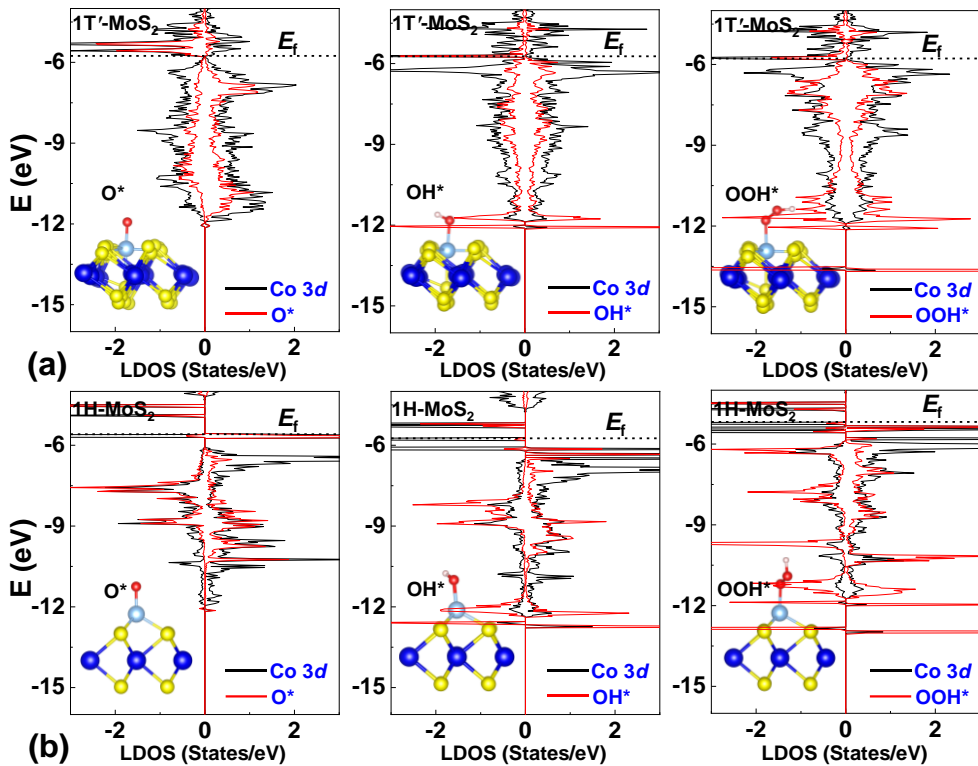


Fig. S11. The local DOS of the anchored Co atoms (black line) and the bonded intermediates (red line) for 1T'-MoS₂ (a) and 1H-MoS₂ (b). The Fermi level is indicated by the horizontal dashed line, with respect to the vacuum level. The relevant intermediates are displayed as insets.

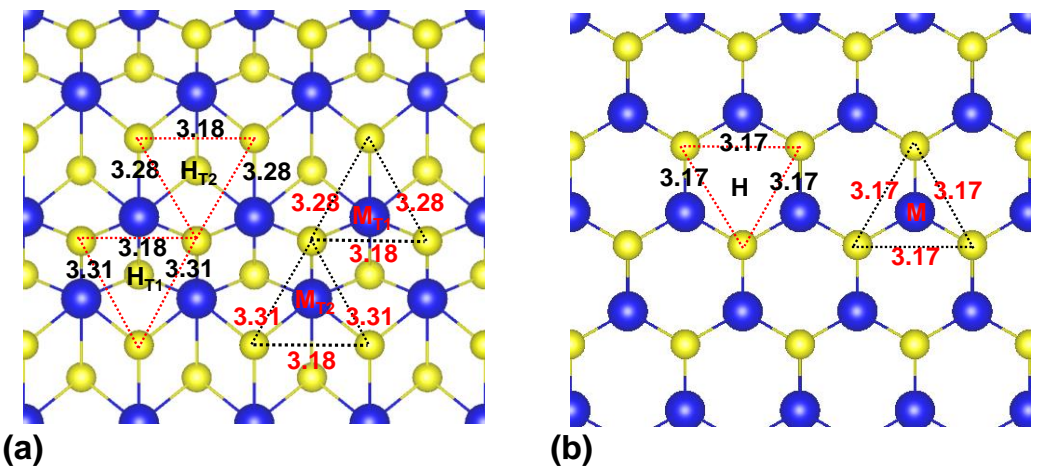


Fig. S12. (a) The S-S distances around the H_{T1}, H_{T2}, M_{T1}, and M_{T2} sites on 1T'-MoS₂.
(b) The S-S distances around H and M sites on 1H-MoS₂.

Note S1: Details on calculating the zero-point energy and TS

In the framework of computational hydrogen electrode model proposed by Nørskov et al.,⁸ the zero-point energy (E_{ZPE}) has been calculated by equation (1):

$$E_{ZPE} = \frac{1}{2} \sum_i h \nu_i \quad (1)$$

The contributions to the free energy resulting from entropy ($-TS$) were calculated by equation (2):

$$-TS = K_B T \sum_i \ln \left(1 - e^{-\frac{h\nu_i}{K_B T}} \right) - \sum_i h \nu_i \left(\frac{1}{e^{\frac{h\nu_i}{K_B T}} - 1} \right) \quad (2)$$

In the equation, h , ν_i , and K_B are the Planck constant, vibrational frequency, and Boltzmann constant, respectively. The zero-point energy and TS values for the gas phase molecules were taken from NIST database, while those for the adsorbates were calculated following equations (1) and (2), respectively. The vibrational frequencies of the adsorbates were calculated by the default algorithm provided by VASP. For H₂O molecule, according to Nørskov et al.,⁸ we used gas-phase H₂O at 0.035 bar as the reference state because at this pressure, gas-phase H₂O is in equilibrium with liquid water at 300 K. In addition, similar to previous works,^{9,10} we only calculated zero-point energy and TS values for the adsorbates on the Co@MoS₂ system, and these values were used for all the other systems, considering that they are insensitive to catalysts.

Note S2: Details on determining theoretical optimum η_{OER} and η_{ORR} as well as constructing activity-volcano plots

In detail, for the OER, the potential determining step (PDS) for Co, Ni, Cu, and Pd@MoS₂ is the second step, thus $\eta^2_{OER} = \Delta G_b/e - 1.23$ V for these systems. On the other hand, for all the other systems (except Mn and Ir@MoS₂) the PDS is the third step, thus $\eta^3_{OER} = \Delta G_c/e - 1.23$ V. In addition, considering that the free energy changes of the third and fourth steps are very close for Ir@MoS₂, the PDS can be approximated as the third step. To obtain the theoretical optimum η_{OER} (the vertex of the activity-volcano plots in Fig. 4c), $\eta^2_{OER} = \eta^3_{OER}$ is required, i.e., $\Delta G_b/e - 1.23 = \Delta G_c/e - 1.23$ and thus $\Delta G_b = \Delta G_c$. Considering $\Delta G_b = \Delta G_{O^*} - \Delta G_{OH^*}$ and $\Delta G_c = \Delta G_{OOH^*} - \Delta G_{O^*}$, as well as the scaling relationship between ΔG_{OOH^*} and ΔG_{OH^*} ($\Delta G_{OOH^*} = 0.91\Delta G_{OH^*} + 3.01$, $R^2 = 0.96$), we have two equations ($\Delta G_b = \Delta G_c$ and $\Delta G_{OOH^*} = 0.91\Delta G_{OH^*} + 3.01$)

but three variables (ΔG_{OH^*} , ΔG_O^* , and ΔG_{OOH^*}). Therefore, to determine the theoretical optimum η_{OER} , we need one additional equation. We noted that previous works^{9, 11, 12} have adopted the equation: $\Delta G_O^* = 2\Delta G_{OH^*}$, which is valid for the (111) surface of various metals¹³. Due to that $\Delta G_a = \Delta G_{OH^*}$ and $\Delta G_b = \Delta G_O^* - \Delta G_{OH^*}$, $\Delta G_O^* = 2\Delta G_{OH^*}$ means that $\Delta G_a = \Delta G_b$. Finally, with the assumption of $\Delta G_a = \Delta G_b$ and $\Delta G_b = \Delta G_c$ (i.e., $\Delta G_a = \Delta G_b = \Delta G_c$), and $\Delta G_{OOH^*} = 0.91\Delta G_{OH^*} + 3.01$, we can obtain the theoretical optimum η_{OER} of 0.21 V and further construct the activity-volcano plots in Fig. 4c.

For the ORR, except Cu, Pd, and Mo@MoS₂ the PDS for all the systems is the last step, i.e., the production of the second H₂O molecule. Moreover, considering that the free energy changes of the second and fourth steps are very close for Cu and Pd@MoS₂, the PDS of both systems can be approximated as the fourth step. Therefore, among all the systems Mo@MoS₂ has the first step as the PDS, while all the other systems can be considered to have the last step as the PDS. Consequently. The theoretical overpotential for the ORR (η_{ORR}) can be written as $\eta_{ORR}^1 = \Delta G_a/e + 1.23$ V = $-\Delta G_d/e + 1.23$ V for Mo@MoS₂ and written as $\eta_{ORR}^4 = \Delta G_d/e + 1.23$ V = $-\Delta G_a/e + 1.23$ V for all the other systems. To obtain the theoretical optimum η_{ORR} (the vertex of the activity-volcano plots in Fig. 4d) and the activity-volcano plots (the solid line in Fig. 4d), $\eta_{ORR}^1 = \eta_{ORR}^4$ is required, which means that ΔG_a is assumed to be equal to ΔG_d . With $\Delta G_a = \Delta G_{OH^*}$ and $\Delta G_d = 4.92 - \Delta G_{OOH^*}$ as well as $\Delta G_{OOH^*} = 0.91\Delta G_{OH^*} + 3.01$, we can obtain the theoretical optimum η_{ORR} of 0.23 V and further construct the activity-volcano plots in Fig. 4d.

References:

1. Q. Zhang and A. Asthagiri, *Catal. Today*, 2019, **323**, 35-43.
2. S. Back, A. R. Kulkarni and S. Siahrostami, *ChemCatChem*, 2018, **10**, 3034-3039.
3. Q. Deng, J. Han, J. Zhao, G. Chen, T. Vegge and H. Anton Hansen, *J. Catal.*, 2021, **393**, 140-148.
4. C. Ataca and S. Ciraci, *J. Phys. Chem. C*, 2011, **115**, 13303-13311.
5. W. Cui, S. Xu, B. Yan, Z. Guo, Q. Xu, B. G. Sumpter, J. Huang, S. Yin, H. Zhao and Y. Wang, *Adv. Electron. Mater.*, 2017, **3**, 1700024.
6. Y. Cheng, Z. Zhu, W. Mi, Z. Guo and U. Schwingenschlögl, *Phys. Rev. B*, 2013, **87**, 100401.
7. J. Ekspong and E. Gracia-Espino, *Adv. Theory Simul.*, 2020, **3**, 1900213.
8. J. K. Nørskov, J. Rossmeisl, A. Logadottir, L. Lindqvist, J. R. Kitchin, T. Bligaard and H. Jónsson, *J. Phys. Chem. B*, 2004, **108**, 17886-17892.
9. G. Gao, E. R. Waclawik and A. Du, *J. Catal.*, 2017, **352**, 579-585.
10. C. Ling, L. Shi, Y. Ouyang, X. C. Zeng and J. Wang, *Nano Lett.*, 2017, **17**, 5133-5139.
11. T. He, S. K. Matta, G. Will and A. Du, *Small Methods*, 2019, **3**, 1800419.
12. J. Wang, Y. Fan, S. Qi, W. Li and M. Zhao, *J. Phys. Chem. C*, 2020, **124**, 9350-9359.
13. A. Kulkarni, S. Siahrostami, A. Patel and J. K. Nørskov, *Chem. Rev.*, 2018, **118**, 2302-2312.